Journal of Luminescence 139 (2013) 52–59

Contents lists available at SciVerse ScienceDirect

Journal of Luminescence

journal homepage: www.elsevier.com/locate/jlumin

Homogeneous broadening effect on temperature dependence of green upconversion luminescence in erbium doped fibers

A. Egatz-Gómez [a,b], Oscar G. Calderón [a,*], Sonia Melle [a], F. Carreño [a], M.A. Antón [a], Elske M. Gort [a,c]

[a] Facultad de Óptica y Optometría, Universidad Complutense de Madrid, Arcos de Jalón 118, Madrid 28037, Spain
[b] Department of Biomedical Engineering, Texas A&M University, College Station, TX 77843, USA
[c] Department of Biomedical Engineering, University of Groningen, 9700 RB Groningen, The Netherlands

ARTICLE INFO

Article history:
Received 31 July 2012
Received in revised form
27 December 2012
Accepted 14 February 2013
Available online 24 February 2013

Keywords:
Upconversion
Erbium doped fiber
Homogeneous broadening
Excited state absorption

ABSTRACT

We study the green upconversion luminescence of Er^{3+} ions in an aluminosilicate optical fiber upon near infrared excitation at 787 nm. The dependence of the upconversion luminescence on temperature has been determined. As temperature drops from room to cryogenic temperatures, the upconversion green emission reaches a maximum around 40 K, and then decreases. A nearly quadratic dependence of the upconversion luminescence with excitation power is found, which is consistent with a sequential stepwise two-photon absorption process. These results have been explained with a semiclassical model that considers the inhomogeneous broadening of the optical transitions due to glass imperfections, and the dependence of the homogeneous linewidth broadening on temperature.

1. Introduction

Upconversion luminescence is a physical process where a high-energy photon is obtained from a material when two or more incident low-energy photons impinge on it. Rare earth (RE) elements are the most important materials which exhibit this behavior due to their unique atomic configuration that results in sharp luminescence emission lines [1]. RE ions have an optically active 4f electron layer shielded by the filled 5s and 5p outer shells. This shielding limits the interaction between the ions and the host material. Among the trivalent RE ions, the erbium ion (Er^{3+}) has been extensively studied because of its ability to emit light within the near-ultraviolet to the near-infrared range upon excitation with infrared light in a number of hosts [2,3]. The absorption and emission peaks can be engineered using different dopant–host combinations [4]. The host material has been shown to strongly modify the luminescence efficiency. Hosts with high phonon energies lead to a reduction of the luminescence efficiency due to non-radiative relaxation [5].

The upconversion process has found a wide range of applications like obtaining green laser emission upon excitation of Er^{3+} by infrared radiation either in crystals [6,7] and fibers [8,9]. Optical waveguides doped with proper ions have been proposed as temperature sensors based on measurements of the intensity ratio of the emission peaks around 530 and 550 nm [10]. More recently, biological applications for Er^{3+} doped nanomaterials such as in-vivo imaging [11–13] and intracellular temperature nanosensors [14] have been proposed. Other emerging applications include three-dimensional volumetric displays [15], and silicon solar cells [16].

The luminescence in materials with several metastable electronic states usually involves a variety of mechanisms. Most of the upconversion two-step processes rely on the ion excitation by ground-state absorption (GSA), subsequent upconversion by excited state absorption (ESA) and/or energy transfer upconversion (ETU), and depletion by luminescence and by multiphonon relaxation [17]. ESA and ETU mechanisms can coexist even though one of them usually dominates over the other. ESA involves only one optically active ion that is promoted to upper levels by sequential resonant absorption of two or more laser photons, and dominates in materials at low-dopant concentrations [18]. ETU is an interionic process that relies on the energy exchange between neighboring ions. It depends strongly on the distance between the ions and predominates at high dopant concentrations.

The dependence of the integrated intensity of the upconversion luminescence signal on the laser excitation intensity follows a power law. The slope of this power law in double-logarithmic representation is indicative of the number of photons involved to excite the emitting state. This slope decreases with increasing excitation power. The influence of the upconversion mechanism and the laser power on this slope have been studied in detail by Pollnau et al. [17].

* Corresponding author. Tel.: +34 91 394 6855.
E-mail address: oscargc@fis.ucm.es (O.G. Calderón).

0022-2313/$ - see front matter © 2013 Elsevier B.V. All rights reserved.
http://dx.doi.org/10.1016/j.jlumin.2013.02.033

The upconversion luminescence of Er^{+3} in many different hosts has been extensively characterized mostly at room temperature due to the interest of erbium doped materials from both a scientific and application point of view [19–25]. Only few works have focused in the behavior of the upconversion signal obtained in these materials at cryogenic temperatures [7,18,26,27]. Typically, as temperature drops from room to cryogenic temperatures, the luminescence intensity increases, reaches a maximum, and then decreases when a further drop of the temperature is achieved. At high temperatures a similar behavior was found by dos Santos et al., where an Er^{3+}/Yb^{3+}-codoped chalcogenide glass was heated from 23 °C to 155 °C [28]. This general trend has been explained on the basis of a competition between nonradiative decays and off-resonance excitation processes. As temperature drops, radiative emission is enhanced due to the decrease of the nonradiative decay rates [29], while the upconversion efficiency diminishes due to a reduction of phonon-assisted absorption [26,28]. Vermelho et al. [26] characterized the upconversion luminescence intensity in erbium-doped tellurite glasses excited at 1540 nm. They observed a maximum green upconversion intensity at 120 K which was explained by the interplay between nonradiative multiphonon relaxations and phonon-assisted absorption at the second step of the stepwise three-photon upconversion process. Golab et al. [27] reported a maximum upconversion emission around 150 K in an Er:YVO_4 crystal pumped with a 808 nm diode laser. They ascribed the reduction in green emission at lower temperatures to the decrease of the $^4I_{9/2}$ level absorption coefficient and the reduction in green emission at higher temperatures to the decrease of the green emission quantum efficiency. Van der Ziel et al. [18] obtained a maximum of the green emission around 90 K in an erbium-doped YF_3 crystal under excitation to level $^4I_{11/2}$. In this case, the reduction in the green emission at lower temperatures resulted from the depopulation of the higher energy stark levels of the $^4I_{11/2}$ manifold, which allows a resonant match for energy transfer upconversion. The effect of temperature on greenupconversion lasing in Er:YALO with excitation around 807 nm ($^4I_{9/2}$) was reported by Scheps [7]. The maximum laser output was achieved at 34 K. Line narrowing was mentioned as a possible mechanism for the laser output quenching below this temperature.

In RE doped glasses the broadening of the absorption and emission line profiles arises from both the thermally excited low-frequency vibrational modes (homogeneous broadening) and the structural disorder of the host material (inhomogeneous broadening) (see the review work of Macfarlane and Shelby [30]). At room temperature the inhomogeneous and homogeneous linewidths are in the same order of magnitude [31,32]. As temperature decreases, the homogeneous broadening decreases highlighting the inhomogeneous character of the material. As a general trend the dependence of the homogeneous linewidth with temperature exhibits a power-law behavior with an exponent ranging from 1 to 2 [33]. At low temperatures tunneling modes contribute to the homogeneous linewidth resulting in a quasilinear dependence with temperature [34,35]. At high temperatures two-phonon Raman processes dominate resulting in a quadratic dependence with temperature [36]. In the intermediate range of temperatures a cross-over is expected [37] and other processes may contribute to the homogeneous width, as for example phonon assisted direct transitions (which also lead to a roughly linear dependence with temperature) [33,38]. The temperature at which this cross-over occurs varies depending on the ion and host considered [37].

Our aim is to experimentally and theoretically analyze the green upconversion luminescence of Er^{3+} ions in an aluminosilicate optical fiber excited at 787 nm. We measure the spectral changes of the upconversion luminescence signal from room temperature to 11 K. To characterize the upconversion mechanism involved we measure the luminescence dependence on the laser excitation power. We develop a semiclassical model that considers the inhomogeneous broadening of the optical transitions due to glass imperfections and we study the influence of different thermal effects on upconversion luminescence.

2. Experimental setup

We experimentally analyze the upconversion green luminescence corresponding to transitions $^4S_{3/2} \rightarrow {}^4I_{15/2}$ and $^2H_{11/2} \rightarrow {}^4I_{15/2}$ of the erbium ions in a single mode Al_2SiO_5-glass-based erbium doped fiber (Liekii, Ltd.) at temperatures from 11 to 300 K (see Er^{3+} ions energy level diagram in Fig. 1). We use the experimental setup depicted in Fig. 2. The fiber has a nominal ion concentration of 6.3×10^{25} ions/m^3 (0.5 mol.%), a peak absorption of 80 dB/m at 1530 nm, a length of 12.7 cm, a nominal mode field diameter (MFD) at 1550 nm of 6.5 μm, a fiber cladding of 245 μm, and a numerical aperture of 0.2. This fiber was rolled around a home-made, 35 mm diameter copper cylinder. The cylinder was affixed to the cold finger of an Edwards cryostat (Coldhead CS2/9) provided with a compressor (Cryodrive 1.5). High vacuum grease was applied to the fiber to ensure a good thermal contact with the cold finger (see photo in Fig. 2). The cold finger temperature was kept constant using a controller from Oxford Instruments (ITC 502) with an accuracy of 0.1 K. The EDF was fusion spliced to standard single mode fibers: at the input of the EDF, a S630-HP (Thorlabs) fiber with operating wavelength 630–860 nm and MFD 4.2 μm at 630 nm, which transmits the excitation power to the EDF; and at the output of the EDF, a 460-HP (Thorlabs) fiber with operating wavelength 450–600 nm and MFD 3.5 μm at 515 nm, which collects the green luminescence. These standard single mode fibers exited the cryostat through a home-made feedthrough, provided with two holes of 125 μm diameter, and were spliced again to undoped connectorized pigtails outside the cryostat with the same characteristics (S630-HP and 460-HP).

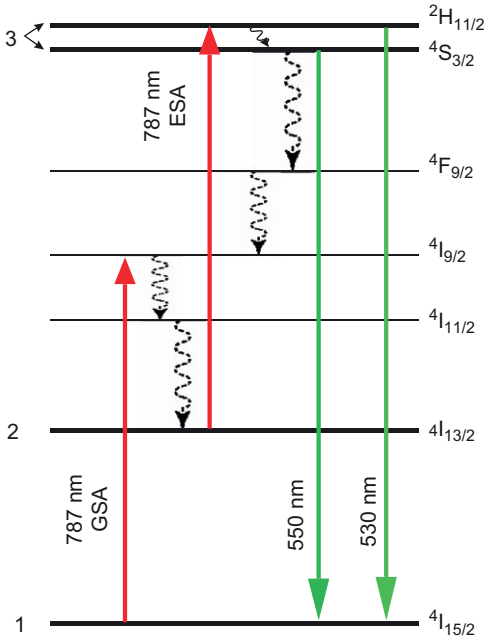

Fig. 1. Partial energy level diagram of Er^{3+} ions. The upward (red) arrows represent laser excitation at 787 nm. The downward solid (green) arrows represent green luminescence emission. Wavy lines represent fast nonradiative decays. GSA: Ground State Absorption; ESA: Excited State Absorption from $^4I_{13/2}$ level. (For interpretation of the references to color in this figure caption, the reader is referred to the web version of this paper.)

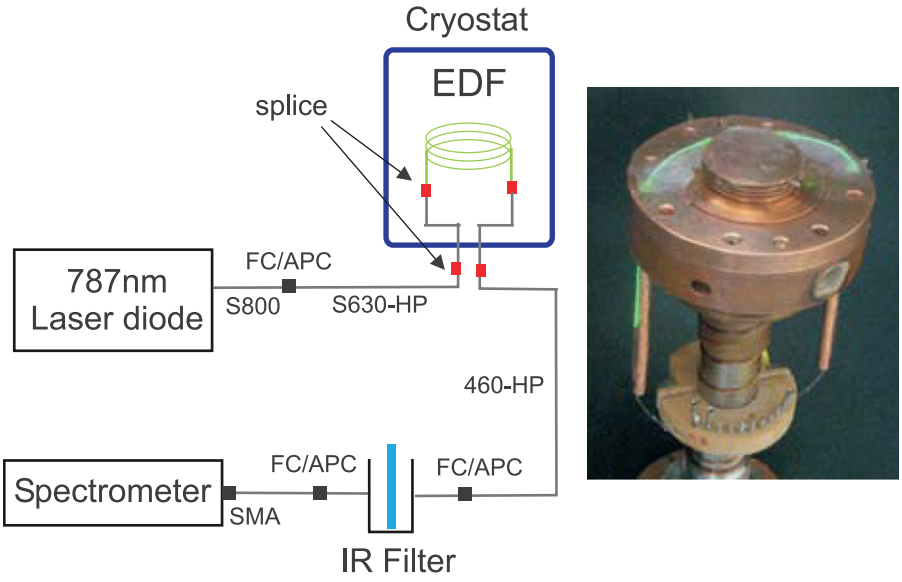

Fig. 2. (Left) Experimental setup used to measure green upconversion luminescence in an erbium doped fiber at cryogenic temperatures. (Right) Photograph of the fiber green luminescence at room temperature.

The EDF is excited with a pigtailed continuous wave (cw) 35 mW laser diode (Power Technology Inc., IQu1A25-787-80G-F2), with emission at 787 nm. The laser was kept at room temperature using a temperature feedback control module. Insertion losses from the laser diode to the S630-HP fiber spliced to the EDF input were estimated to be 0.16. We measured the green fluorescence spectra with a USB650-Red Tide spectrometer (Ocean Optics) with a spectral resolution of 1 nm using integration times between 5 and 15 s, and averaging 5 to 50 scans depending on the range of input powers used. In order to compare the spectra obtained at different excitation powers we normalized all the spectra with their respective integration time. At the output of the EDF and outside the cryostat we used a U-bench with a dichroic IR filter (50% cutoff at 615 nm) to avoid hindering of the green emission detection by the spectrometer due to the laser signal. In order to work in the low power regime we used a 99/1 splitter at the laser output (Thorlabs, FC830-99B-4FC/APC-SP). One percent of the input beam was sent directly to a switchable-gain amplified InGaAs photodetector (Thorlabs, PDA10CS) as a reference for the input power. The other 99% was sent directly to the S630-HP fiber connected to the EDF input. Insertion losses from the 99% arm of the splitter output to the S630-HP fiber connected to the EDF input were negligible.

We also measured the room temperature input–output laser power curve to characterize the fiber physical parameters: room temperature linear absorption coefficient, room temperature saturation power, and ratio between the ground and the excited state absorption cross-sections. Measurements were done outside the cryostat to circumvent the strong attenuation of the laser signal through the 460-HP fiber used in our cryostat setup. We illuminated the fiber through the 99% coupling end of a 99/1 splitter connected to the 787 nm laser diode. We used two identical photodetectors (Thorlabs, PDA10CS), one at the 1% output of the splitter and the other one at the EDF end. We recorded the input and output voltages simultaneously with a digital oscilloscope (Agilent, DSO9104A) and calibrated the power–voltage conversion with a power meter (Thorlabs, PM122).

3. Results

Fig. 3 shows the upconversion emission spectra between 510 and 590 nm, at temperatures from 11 to 300 K, for a 29 mW

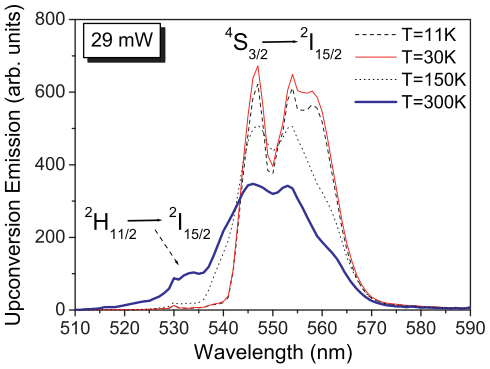

Fig. 3. Upconversion luminescence spectra at different temperatures for a fixed excitation power of 29 mW at 787 nm.

excitation power resonant with level $^4I_{9/2}$ (see Fig. 1). We observe two different green luminescence bands on the room temperature emission spectrum (thick solid line): one around 530 nm, which is attributed to transition $^2H_{11/2} \rightarrow {}^4I_{15/2}$, and the other one around 550 nm $^4S_{3/2} \rightarrow {}^4I_{15/2}$ ascribed to the transition. When the temperature drops to 150 K, the luminescence band around 530 nm is not longer noticeable (see dotted line). This emission band is only revealed at high temperatures because the $^2H_{11/2}$ level is thermally populated due to the small energy separation between $^2H_{11/2}$ and $^4S_{3/2}$ levels [21,28,39]. The luminescence around 550 nm increases when decreasing temperature: at 30 K (see thin solid line) the peak enhancement around 547 nm relative to room temperature is twofold; however, below 30 K the spectrum decreases (see dashed line corresponding to 11 K).

We analyze in detail the dependence of the upconversion emission with temperature between 11 and 300 K. To this end we compute the total upconversion emission intensity by integrating the emission intensity from 510 to 590 nm. The results are plotted in Fig. 4 for an excitation power of 29 mW (circles) and 8.3 mW (squares). We observe that as temperature drops from 300 K, the integrated emission intensity increases reading a maximum around 40 K. Below this optimum temperature a monotonic decrease in upconversion emission becomes evident. The temperature dependence of the intensity in our experiments follows a trend similar to the studies by Vermelho et al. [26],

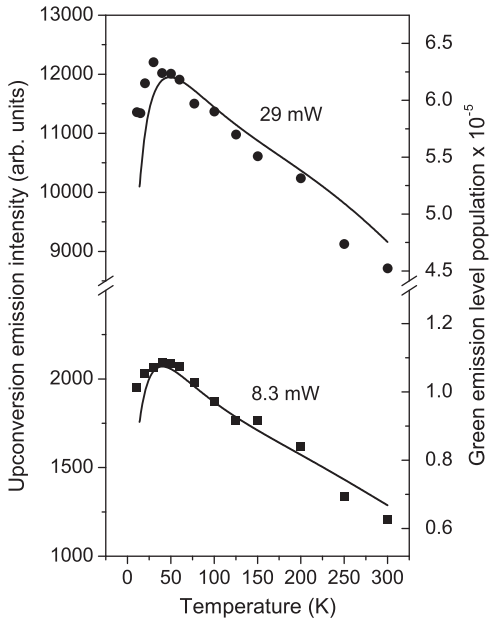

Fig. 4. Integrated upconversion emission intensity in left axis (symbols) and simulated green emission level population ρ_{33} (Eq. (18)) in right axis (lines) versus temperature for two excitation powers: 29 mW (circles) and 8.3 mW (squares). In Eq. (18) we use the excitation field intensity at the end of the EDF, i.e., $I(z=L)$ calculated using Eq. (22).

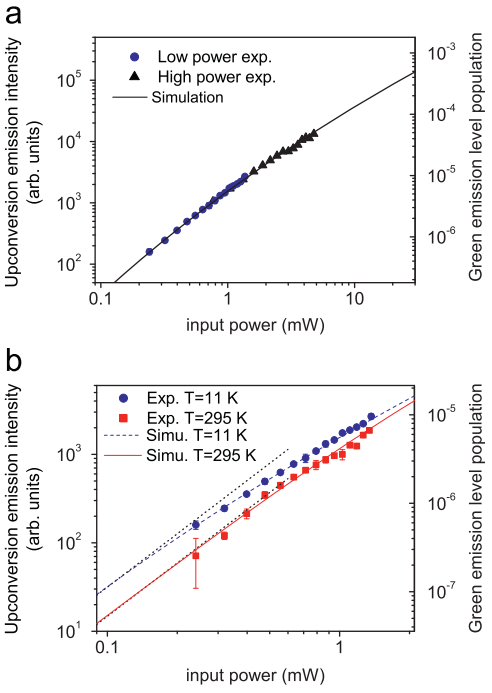

Fig. 5. Upconversion emission intensity data (left axis, symbols) and simulated green emission level population ρ_{33} (Eq. (18)) (right axis, solid and dashed lines) versus excitation power. (a) Low power region (circles), high power region (triangles), and simulated curve (solid line) at $T=11$ K. (b) Low power region at $T=295$ K (squares) and $T=11$ K (circles), and simulated curves at $T=295$ K (solid line) and $T=11$ K (dashed line). Power law curves with exponent 2 have been added as a guide for the eye (dotted lines). In Eq. (18) we use the excitation field intensity at the end of the EDF, i.e., $I(z=L)$ calculated using Eq. (22).

Golab et al. [27], and dos Santos et al. [28], which were performed at different excitation wavelengths and host materials, and where the dependence was explained in terms of the competition between two thermal effects, as discussed previously in the introduction. The proposed mechanisms for this behavior in our case are discussed along the following sections.

The dependence of the integrated upconversion green luminescence on the excitation power at 11 K is plotted in Fig. 5(a) in a log–log representation (symbols). We observe a nearly quadratic dependence at low excitation powers indicating that a two-photon upconversion excitation scheme takes place. At higher powers this dependence saturates due to nonlinear absorption. In Fig. 5(b) we compare the data shown on Fig. 5(a) for the low power region (circles) to measurements performed at room temperature (squares). Both curves exhibit a similar trend. However, the exponent of the power law at room temperature is closer to 2 than the exponent of the power law at 11 K. Power law curves with exponent 2 have been added as a guide for the eye (see dotted lines). In the low power limit, i.e., for powers below the saturation power, this slope is indicative of the number of photons required for the upconversion process. The deviation from the quadratic behavior can be ascribed to a reduction of the saturation power at cryogenic temperatures [38].

4. Model

In order to theoretically interpret the experimental findings, we resort to model the upconversion process in the EDF within a semiclassical framework. Let us consider an inhomogeneously broadened collection of erbium ions in an aluminosilicate glass host, excited by a laser field $\mathcal{E}$ with a near-infrared carrier frequency ω (787 nm)

$$\mathcal{E}(z,t)=\tfrac{1}{2}E(z,t)e^{-i\omega t}+c.c \quad ., \tag{1}$$

where *c.c.* stands for complex conjugation and E is the slowly varying amplitude of the laser field. The Er^{+3} concentration of our fiber is 0.5 mol.%. At these dopant concentrations it is generally considered that ESA dominates over ETU [18]. The energy levels of the erbium ions and the upconversion mechanism (ESA) considered in this model are shown in Fig. 1 [39]. Due to the high phonon energies in silica-based glasses, multiphonon decay is the dominant relaxation process for all the excited states in this host except for the metastable level $^4I_{13/2}$, which exhibits a purely radiative decay [40].

The temperature dependence of the multiphonon relaxation rate $\Gamma^{pho}(T)$ of an excited state can be estimated from the energy-gap law

$$\Gamma^{pho}(T)=\Gamma^{pho}(0)[1-e^{-\hbar\omega_{max}/(k_BT)}]^{-p}. \tag{2}$$

Here $\Gamma^{pho}(0)=k\exp[-\xi(\Delta E-2\hbar\omega_{max})]$ is the multiphonon relaxation rate at 0 K, and $\hbar\omega_{max}$ is the highest optical phonon energy. The characteristic parameters of silica glasses are $k=9\times10^7\ s^{-1}$, $\xi=4.7\times10^{-3}$ cm, and $\hbar\omega_{max}\simeq1000\ cm^{-1}$ [40]. ΔE is the energy difference between an excited level and its next lower level, $p=\Delta E/(k_BT)$ is the minimum number of phonons involved in the relaxation, and k_B is the Boltzmann constant. We use the energy gaps ΔE of Ref. [40].

Let us describe the upconversion mechanism indicated in Fig. 1. In the first step one photon excites the Er^{+3} ion from the $^4I_{15/2}$ to the $^4I_{9/2}$ level (GSA) which relaxes non-radiatively to the lower levels $^4I_{11/2}$ and $^4I_{13/2}$. In the second step, the ion absorbs another photon (ESA), it is promoted from the metastable level $^4I_{13/2}$ (level 2, see Fig. 1) to the $^2H_{11/2}$ level, and from this level decays to the $^4S_{3/2}$ level. Due to the small energy difference between $^2H_{11/2}$ and $^4S_{3/2}$ levels, the upper level $^2H_{11/2}$ can be thermally populated from the $^4S_{3/2}$ level. Finally, radiative decay from these two levels to the ground state $^4I_{15/2}$ leads to green luminescence. Hereafter, the $^2H_{11/2}$ and $^4S_{3/2}$ levels will be collectively referred to as the green emission level (level 3, see Fig. 1).

The inhomogeneous broadening of the atomic transitions due to glass imperfections is introduced as follows. The medium is formed by ion-packets with a ground state transition frequency ω_n^{G} distributed around the central frequency ω_0^{G}, and an excited state transition frequency ω_m^{E} distributed around ω_0^{E} (where n and m indicate the packet numbering). Following a semiclassical approach, the equations of motion of the relevant populations and coherences corresponding to the (n, m)-th ion-packet in the rotating frame are given as

$$\frac{\partial\rho_{22}^{(n,m)}}{\partial t}=\Gamma_{32}^{pho}\rho_{33}^{(n,m)}-\Gamma_{21}\rho_{22}^{(n,m)} -i\left(\frac{\mu_{\mathrm{G}}E^*}{2\hbar}\rho_{\mathrm{G}}^{(n,m)}-c.c.\right)+i\left(\frac{\mu_{\mathrm{E}}E^*}{2\hbar}\rho_{\mathrm{E}}^{(n,m)}-c.c.\right), \tag{3}$$

$$\frac{\partial\rho_{33}^{(n,m)}}{\partial t}=-(\Gamma_{32}^{pho}+\Gamma_{31})\rho_{33}^{(n,m)}-i\left(\frac{\mu_{\mathrm{E}}E^*}{2\hbar}\rho_{\mathrm{E}}^{(n,m)}-c.c.\right), \tag{4}$$

$$\frac{\partial\rho_{\mathrm{G}}^{(n,m)}}{\partial t}=-(\gamma^{\mathrm{G}}+i\Delta_n)\rho_{\mathrm{G}}^{(n,m)}+i\frac{\mu_{\mathrm{G}}E}{2\hbar}\rho_{11}^{(n,m)}, \tag{5}$$

$$\frac{\partial\rho_{\mathrm{E}}^{(n,m)}}{\partial t}=-(\gamma^{\mathrm{E}}+i\Delta_m)\rho_{\mathrm{E}}^{(n,m)}+i\frac{\mu_{\mathrm{E}}E}{2\hbar}\rho_{22}^{(n,m)}, \tag{6}$$

where $\rho_{22}^{(n,m)}$ is the population of the metastable level, $\rho_{33}^{(n,m)}$ is the population of the green emission level, and $\rho_{\mathrm{G}}^{(n,m)}$ and $\rho_{\mathrm{E}}^{(n,m)}$ are the atomic coherences of the GSA and the ESA transitions, respectively. Here $\Delta_n=\omega_n^{\mathrm{G}}-\omega$ is the detuning between the GSA transition frequency and the frequency of the excitation field, and $\Delta_m=\omega_m^{\mathrm{E}}-\omega$ is the detuning between the ESA transition frequency and the frequency of the excitation field. Here μ_{G} and μ_{E} stand for the dipolar moment of the GSA and ESA transition, respectively. Γ_{21} and Γ_{31} are the population radiative decay rates. We assume that the change of these radiative decay rates with temperature is negligible because this variation does not significantly change the results, as we will discuss later in next section. In this work we consider typical radiative decay rates for aluminosilicate glasses at room temperature: $\Gamma_{21}=130\ \mathrm{s}^{-1}$, and $\Gamma_{31}=1280\ \mathrm{s}^{-1}$ [40]. Γ_{32}^{pho} is the non-radiative multiphonon relaxation decay rate between levels 3 and 2,

$$\Gamma_{32}^{pho}(T)=\Gamma_{32}^{pho}(0)[1-e^{-\hbar\omega_{max}/(k_BT)}]^{-p}, \tag{7}$$

where the energy gap between the excited level $^4\mathrm{S}_{3/2}$ and its next lower level ($^4\mathrm{F}_{9/2}$) is $\Delta E=3000\ \mathrm{cm}^{-1}$, so that $\Gamma_{32}^{pho}(0)=9.42\times10^5\ \mathrm{s}^{-1}$ [40]. The dephasing rates γ^{G} and γ^{E} are the homogenous linewidth of the GSA and the ESA transitions, respectively. It is generally accepted that the homogeneous linewidth depends on temperature following a power law with an exponent between 1 and 2 [30]

$$\gamma^{\mathrm{G}}(T)\sim T^q \quad\text{and}\quad \gamma^{\mathrm{E}}(T)\sim T^{q'}. \tag{8}$$

The population of the ground level is computed considering a closed system, i.e., $\rho_{11}^{(n,m)}=1-\rho_{22}^{(n,m)}-\rho_{33}^{(n,m)}$. The coherences and populations attained in steady-state read as

$$\rho_{\mathrm{G}}^{(n,m)}=\frac{i\mu_{\mathrm{G}}E\rho_{11}^{(n,m)}}{2\hbar\gamma^{\mathrm{G}}(1+i\delta_n)}, \tag{9}$$

$$\rho_{\mathrm{E}}^{(n,m)}=\frac{i\mu_{\mathrm{E}}E\rho_{22}^{(n,m)}}{2\hbar\gamma^{\mathrm{E}}(1+i\delta_m)}, \tag{10}$$

$$\rho_{22}^{(n,m)}=\frac{\frac{I}{I^{sat}}}{1+\delta_n^2+\frac{I}{I^{sat}}+\frac{\beta\Gamma_{31}}{\Gamma_{32}^{pho}+\Gamma_{31}}\frac{1+\delta_n^2}{1+\delta_m^2}\frac{I}{I^{sat}}+\frac{\beta\Gamma_{21}}{\Gamma_{32}^{pho}+\Gamma_{31}}\frac{1}{1+\delta_m^2}\left(\frac{I}{I^{sat}}\right)^2}, \tag{11}$$

$$\rho_{33}^{(n,m)}=\frac{\frac{\beta\Gamma_{21}}{\Gamma_{32}^{pho}+\Gamma_{31}}\left(\frac{I}{I^{sat}}\right)^2}{(1+\delta_n^2)(1+\delta_m^2)+(1+\delta_m^2)\frac{I}{I^{sat}}+\frac{\beta\Gamma_{31}}{\Gamma_{32}^{pho}+\Gamma_{31}}(1+\delta_n^2)\frac{I}{I^{sat}}+\frac{\beta\Gamma_{21}}{\Gamma_{32}^{pho}+\Gamma_{31}}\left(\frac{I}{I^{sat}}\right)^2}, \tag{12}$$

where $\delta_n=\Delta_n/\gamma^{\mathrm{G}}$ and $\delta_m=\Delta_m/\gamma^{\mathrm{E}}$ are the normalized detunings of the GSA and ESA transition, respectively. Here I is the excitation intensity and I^{sat} is the saturation intensity of the GSA transition

$$I^{sat}=\frac{c\epsilon_0\hbar^2\Gamma_{21}\gamma^{\mathrm{G}}}{\mu_{\mathrm{G}}^2}. \tag{13}$$

This saturation intensity indicates a threshold above which the absorption, otherwise independent of input intensity, decreases with increasing input intensity. The parameter β is the ratio between the absorption cross-sections of the ESA (σ_{E}) and the GSA transitions (σ_{G}) which are comparable in magnitude [41]

$$\beta=\frac{(\mu_E^2/\gamma^{\mathrm{E}})}{(\mu_G^2/\gamma^{\mathrm{G}})}=\frac{\sigma_{\mathrm{E}}}{\sigma_{\mathrm{G}}}. \tag{14}$$

This parameters is indicative of the efficiency of the upconversion processes. As we mentioned above the non-radiative multiphonon relaxation decay rate Γ_{32}^{pho} differs from the radiative decay rates Γ_{21} and Γ_{31} in several order of magnitude which allows us to simplify the steady-state populations (11) and (12) as follows:

$$\rho_{22}^{(n,m)}\cong\frac{\frac{I}{I^{sat}}}{1+\delta_n^2+\frac{I}{I^{sat}}}, \tag{15}$$

$$\rho_{33}^{(n,m)}\cong\frac{\frac{\beta\Gamma_{21}}{\Gamma_{32}^{pho}+\Gamma_{31}}\left(\frac{I}{I^{sat}}\right)^2}{(1+\delta_m^2)\left(1+\delta_n^2+\frac{I}{I^{sat}}\right)}. \tag{16}$$

To study the green upconversion emission we compute the total population of the green emission level integrating over the inhomogeneous profile of the two step transitions

$$\rho_{33}=\iint d\omega_m^{\mathrm{E}}G(\omega_m^{\mathrm{E}})\,d\omega_n^{\mathrm{G}}H(\omega_n^{\mathrm{G}})\,\rho_{33}^{(n,m)}, \tag{17}$$

$H(\omega_n^{\mathrm{G}})$ being the normalized inhomogeneous distribution of the ground state transition frequency ω_n^{G}, centered at ω_0^{G} and with a half width at half maximum (HWHM) of γ_I^{G}. The normalized inhomogeneous distribution $G(\omega_m^{\mathrm{E}})$ of the excited state transition frequency has a half width at half maximum γ_I^{E}. Analytical results can be derived from Eq. (17) if we assume that both inhomogeneous distributions follow a Lorentzian function. Further, we consider that $\omega\simeq\omega_0^{\mathrm{G}}\simeq\omega_0^{\mathrm{E}}$. The total population of the green emission level becomes

$$\rho_{33}=\frac{(I(z)/I^{sat}(T))^2\frac{\beta\Gamma_{21}}{\Gamma_{32}^{pho}(T)+\Gamma_{31}}}{\sqrt{1+I(z)/I^{sat}(T)}(\gamma_I^{\mathrm{G}}/\gamma^{\mathrm{G}}(T)+\sqrt{1+I(z)/I^{sat}(T)})(1+\gamma_I^{\mathrm{E}}/\gamma^{\mathrm{E}}(T))}. \tag{18}$$

As can be seen, the total population of the green emission level depends on temperature through the homogeneous linewidths γ^{E} and γ^{G} (and therefore through I^{sat}), and the non-radiative multiphonon relaxation decay rate Γ_{32}^{pho}. Furthermore, ρ_{33} depends on the excitation intensity I that could vary along the fiber. Then, we calculate the propagation of the excitation field through the medium in the slowly varying approximation through the spatial part of the wave equation which reads

$$\frac{\partial E}{\partial z}+i\frac{\omega}{c}E=\frac{i\omega}{2\epsilon_0}P, \tag{19}$$

where the source term stands for the macroscopic polarization of the atomic medium oscillating at the excitation frequency which is given by

$$P = 2N \iint d\omega_m^{\mathrm{E}} G(\omega_m^{\mathrm{E}})\, d\omega_n^{\mathrm{G}} H(\omega_n^{\mathrm{G}})(\mu_{\mathrm{G}} \rho_G^{(n,m)} + \mu_{\mathrm{E}} \rho_E^{(n,m)}), \tag{20}$$

and N is the total number of ions. We insert the steady-state values of ρ_{G} and ρ_{E} in Eq. (20). From Eqs. (19) and (20), we obtain the following propagation equation for the excitation field intensity

$$\frac{\partial I}{\partial z} = -\alpha_0 I \iint d\omega_m^{\mathrm{E}} G(\omega_m^{\mathrm{E}})\, d\omega_n^{\mathrm{G}} H(\omega_n^{\mathrm{G}}) \left[\frac{\rho_{11}^{(n,m)}}{1+\delta_n^2} + \beta \frac{\rho_{22}^{(n,m)}}{1+\delta_m^2} \right], \tag{21}$$

where $\alpha_0(T) = N\mu_{\mathrm{G}}^2 \omega/(\hbar c \epsilon_0 \gamma^{\mathrm{G}}(T))$ stands for the homogeneous unsaturated absorption coefficient of the GSA transition. In order to evaluate the propagation of the excitation field we neglect the population of the green emission level, i.e., $\rho_{11}^{(n,m)} \simeq 1 - \rho_{22}^{(n,m)}$. By using the steady-state value of $\rho_{22}^{(n,m)}$ and performing the integral over the inhomogeneous frequency profiles, Eq. (21) reduces to

$$\frac{\partial I}{\partial z} = \frac{-\alpha_0(T) I \left(1 + \beta \dfrac{I/I^{sat}(T)}{1+\gamma_I^{\mathrm{E}}/\gamma^{\mathrm{E}}(T)} \right)}{\sqrt{1+I/I^{sat}(T)}(\gamma_I^{\mathrm{G}}/\gamma^{\mathrm{G}}(T) + \sqrt{1+I/I^{sat}(T)})}. \tag{22}$$

5. Discussion

We characterize the physical parameters of our EDF at room temperature. We measure the transmittance of the 787 nm signal along the EDF by placing the EDF outside of the cryostat. The results are shown in Fig. 6. The slope of the input–output power curve decreases with input power indicating a transmission reduction with input power as typically occurs in systems governed by ESA. By fitting the input–output power curve to Eq. (22) we obtain $\beta = 3.2$, the room temperature unsaturated absorption coefficient $\alpha_0(300\ \mathrm{K}) = 0.06\ \mathrm{cm}^{-1}$, and the room temperature GSA saturation power $P^{sat}(300\ \mathrm{K}) = 3$ mW, where $P^{sat} = A_{eff} I^{sat}$, A_{eff} being the effective doping area of the fiber. Here we have assumed that the homogeneous width at room temperature is similar to the inhomogeneous linewidth [31,32].

We use Eq. (18) to analyze the dependence of the population of the green emission level with temperature in order to reproduce the green upconversion emission intensity variation found in the experiments (see Fig. 4). We consider different thermal mechanisms that may modify the green upconversion emission intensity.

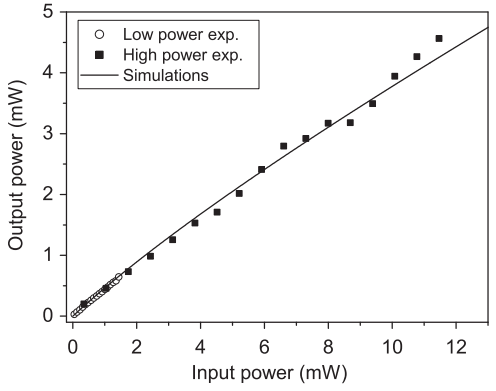

Fig. 6. Experimental transmission of the 787 nm signal along the EDF at room temperature: low power region (open circles), high power region (squares). Fit to Eq. (22) (solid curve). Insertion losses: from the 99/1 divisor to the EDF, 0.7 (low power region); from the diode laser to the EDF, 0.23 (high power region). For this measurement the EDF was placed outside the cryostat.

5.1. Multiphonon relaxation

The first mechanism that one could expect to be affected by temperature is the multiphonon relaxation (see Eq. (7)). In fact, the average number of phonons decreases as temperature drops, which produces a decrease of nonradiative multiphonon decays. Therefore, an increase of population is expected upon lowering the temperature. To test if this phenomenon explains the experimental results we plot in Fig. 7 (solid curve) the population ρ_{33} (Eq. (18)) taking into account the temperature dependence of the multiphonon relaxation rate $\Gamma_{32}^{pho}(T)$ (see Eq. (7)). To this end we consider that $\gamma^{\mathrm{G}} \simeq \gamma_I^{\mathrm{G}}$, and $\gamma_{\mathrm{E}} \simeq \gamma_I^{\mathrm{E}}$ at all temperatures. For the sake of simplicity we also consider that the excitation intensity is the one at the input of the fiber [$I(z=0)$]. We see that the change in the population due to the variation of the multiphonon relaxation with temperature is rather small (2%). This is attributed to the high energy of phonons in this type of host, which limits the temperature variation of $\Gamma_{32}^{pho}(T)$. In fact, $\Gamma_{32}^{pho}(T)$ changes from $9.6 \times 10^5\ \mathrm{s}^{-1}$ at room temperature to $9.42 \times 10^5\ \mathrm{s}^{-1}$ at 0 K. Because the influence of temperature on the multiphonon relaxation is negligible (solid curve), this effect cannot explain our experimental findings.

5.2. Radiative decays

As we have mentioned above, the radiative decay rates Γ_{21} and Γ_{31} may change with temperature. Regarding Γ_{21}, previous work has shown a slowly decreasing trend (around 15%) of the metastable $^4I_{13/2}$ level lifetime with increasing temperature [40,42]. This decrease was attributed to the faster radiative decay rates of the higher-lying crystal-field levels of the $^4I_{13/2}$ manifold, which are thermally populated.

Concerning Γ_{31}, we consider that the upper level $^2H^{11/2}$ is thermally populated from level $^4S^{3/2}$ due to the small energy difference (around 800 cm^{-1}). Then the population in the $^2H^{11/2}$ and the $^4S^{3/2}$ levels can be treated as a closed system in thermal equilibrium. We compute from our experimental upconversion luminescence spectra (see Fig. 3) the ratio between the luminescence intensity of both levels $L(^2H_{11/2})/L(^4S_{3/2})$ at different

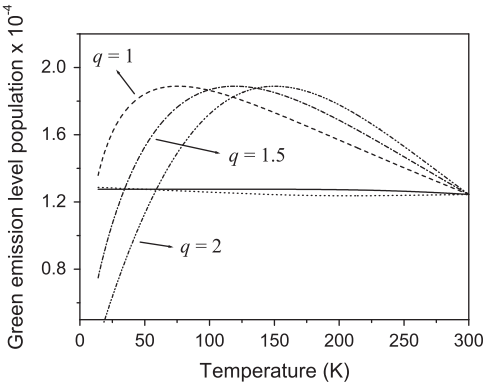

Fig. 7. Dependence of the green emission level population ρ_{33} (Eq. (18)) on temperature: assuming that temperature only affects the multiphonon relaxation processes (solid curve), assuming that temperature affects multiphonon relaxation and radiative decay rates (dotted curve); and assuming that temperature affects multiphonon relaxation and homogeneous broadening, for different exponents $q=1$ (dashed curve), 1.5 (dashed-dotted curve) and 2 (dashed-dotted-dotted curve). We use the parameters that characterize our fiber: $P^{sat}(300\ \mathrm{K}) = 3$ mW, $\beta = 3.2$. We also consider insertion losses 0.16, and input power 29 mW.

temperatures. This ratio is given by

$$\frac{L(^2H_{11/2})}{L(^4S_{3/2})} = \frac{g_H}{g_S}\frac{\Gamma_{31}(^2H_{11/2})}{\Gamma_{31}(^4S_{3/2})}e^{-\Delta E/(k_B T)}, \quad (23)$$

where g_H and g_S are the level degeneracies and $\Gamma_{31}(^2H_{11/2})$ and $\Gamma_{31}(^4S_{3/2})$ are the radiative decay rates of the $^2H_{11/2}$ and $^4S_{3/2}$ levels, respectively. ΔE is the energy gap between both levels. By fitting our experimental data to Eq. (23) we obtained $\Gamma_{31}(^2H_{11/2})/\Gamma_{31}(^4S_{3/2}) = 2$ and $\Delta E = 755\ cm^{-1}$. Then, we estimated a variation of the effective radiative decay rate of the green level to the ground level Γ_{31} with temperature of around 7%. A similar variation can be estimated for Er^{+3} ions in a fluorozirconate glass [42].

To test if the estimated variation of the decay rates Γ_{21} and Γ_{31} explains the upconversion emission found in the experiments we plot in Fig. 7 $\rho_{33}\ \Gamma_{31}/\Gamma_{31}(300\ K)$ as a function of temperature (see dotted curve). We observe that the green emission level population does not significantly change when the radiative decay rates Γ_{21} and Γ_{31} exhibit the temperature variation discussed above. So this effect is not relevant for our results.

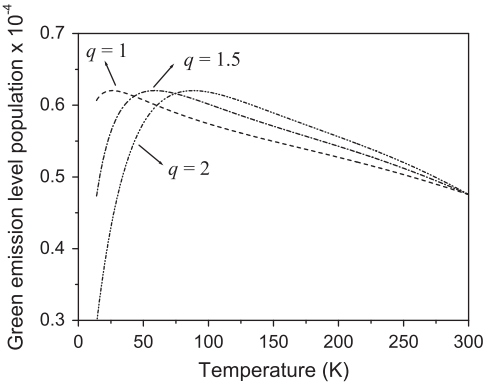

Fig. 8. Dependence of the green emission level population ρ_{33} (Eq. (18)) on temperature assuming that temperature affects multiphonon relaxation, homogeneous broadening, and considering the propagation of the excitation field along the fiber (Eq. (22)) for different exponents $q=1$ (dashed curve), 1.5 (dashed-dotted curve) and 2 (dashed-dotted-dotted curve). We use the parameters that characterize our fiber: $P^{sat}(300\ K)=3$ mW, $\beta=3.2$. We also consider insertion losses 0.16, and input power 29 mW.

5.3. Homogeneous broadening

Another mechanism affected by temperature is the homogenous broadening. The homogeneous linewidth can be affected by tunneling modes, direct phonon, two-phonon Raman and multiphonon relaxation processes. Note that the temperature variation of the homogeneous linewidths can be translated into a temperature variation of the respective cross-sections. We study the role of the homogenous linewidths $\gamma^G(T)$ and $\gamma^E(T)$ temperature variation in the upconversion luminescence. We assume that the homogeneous width at room temperature is similar to the inhomogeneous linewidth [31,32]. As we mentioned in the Introduction, the homogeneous linewidth depends on temperature following a power law with an exponent between 1 and 2. Let us assume for the sake of simplicity the same power-law dependence with temperature for both homogeneous linewidths: $\gamma^G(T)/\gamma_I^G = \gamma^E(T)/\gamma_I^E = (T/300)^q$, being q an exponent between 1 and 2. We plot in Fig. 7 the population ρ_{33} for different values of the exponent q (see dashed, dashed-dotted and dashed-dotted-dotted curves). These curves exhibit a large variation of the population with temperature and a maximum value for intermediate temperatures, whose position is q-dependent. These curves follow a trend similar to the experimental curves, which indicates that the variation of the homogeneous linewidth with temperature plays a major role in our experimental findings. An accurate fit to the experimental data presented in Fig. 4 is not achievable by using q as fitting parameter which indicates that another phenomenon should be taken into account.

5.3.1. Attenuation of the excitation field

In order to reproduce more accurately the experimental results plotted in Fig. 4, we consider that most of the measured luminescence is coming from the output of the EDF. Therefore, in order to calculate the population of the green emission level, we must take into account the attenuation of the excitation laser through the EDF, that is, we must consider that the excitation intensity appearing in Eq. (18) is that obtained at the end of the fiber $I(z=L)$ calculated by solving Eq. (22). In Fig. 8 we plot the population ρ_{33} by considering the attenuation of the excitation beam through the EDF for the same parameters as in Fig. 7 and for $\alpha_0(300\ K) = 0.06\ cm^{-1}$ which corresponds to our experimental fiber. We observe that the effect of considering the propagation of the excitation field through the EDF leads to a decrease of the green emission level population, a shift in the curve maxima to lower temperatures, and a change in the curve shape.

We fit the experimental upconversion emission intensity shown in Fig. 4 to the calculated ρ_{33} that accounts for the attenuation of the excitation laser through the EDF using the exponent q as fitting parameter. The simulated temperature behavior of the green emission intensity shows a good agreement with the experimental data for $q=1.35$ (see lines in Fig. 4). This exponent is similar to the one found for the $^4I_{13/2}$–$^4I_{15/2}$ transition in aluminosilicate glasses [33]. These results allow us to explain the temperature dependence of the integrated upconversion signal in terms of the combined effects of homogeneous broadening and the attenuation of the exciting field during its propagation along the fiber.

Taking into account this effect we have also simulated the dependence of the green emission intensity ρ_{33} with input power using Eq. (18) for $I(z=L)$. The results are shown in Fig. 5 with solid and dashed lines. A good agreement between simulations and experimental data is found. At low excitation powers, a quadratic dependence of the population of the green emission level with the excitation intensity is found ($\rho_{33} \sim I^2$) (see Eq. (18)). However, in the limit of very high excitation powers, a linear dependence arises ($\rho_{33} \sim I$), which is responsible for the saturation of the slope shown in Fig. 5(a). Furthermore, simulations yield a power law exponent at 11 K slightly lower than 2, whereas the exponent is approximately 2 at room temperature, which matches our experimental findings (see Fig. 5(b)). The excitation powers used in Fig. 5(b) (from 0.24 to 1.4 mW) are smaller than the saturation power at room temperature (3 mW), which confirms the quadratic power law found. On the other hand, the saturation power decreases as the temperature drops following the behavior of the homogeneous linewidth γ^G (see Eq. (13)). We estimate a saturation power of 0.04 mW at 11 K. Since the excitation power used exceeds the saturation value, the power law deviates from its quadratic form due to nonlinear absorption.

6. Conclusions

We experimentally and theoretically studied the green upconversion luminescence of Er^{3+} ions in an aluminosilicate optical fiber upon near infrared excitation at 787 nm. We analyzed the temperature behavior of the upconversion emission intensity. As temperature drops from room to cryogenic temperatures, an

enhancement of upconversion emission takes place with a maximum intensity around 40 K. Below this optimum temperature, the green emission decreases. In order to characterize the upconversion mechanism involved we measured the luminescence dependence on excitation power. We found a nearly quadratic dependence, which is consistent with a sequential stepwise two-photon absorption process.

We developed a semiclassical model that considers a collection of erbium ions in an aluminosilicate glass host excited by a laser field with a near-infrared carrier frequency resonant with the GSA transition $^4I_{15/2} \rightarrow {}^4I_{9/2}$ and ESA transition $^4I_{13/2} \rightarrow {}^4I_{15/2}$. The inhomogeneous broadening of the optical transitions due to glass imperfections was taken into consideration. We analytically calculated the population of the green emission level, which is proportional to the green upconversion luminescence. We analyzed the influence of different thermal effects on upconversion luminescence. We found that the effect of the temperature variation of the multiphonon relaxation on upconversion emission is negligible. Another thermal effect considered was the homogeneous broadening of the GSA and ESA transitions. This phenomenon explains our experimental findings. A more accurate simulated result was obtained by taking into account the attenuation of the excitation laser through the erbium doped fiber and using the laser power at the end of the fiber to calculate the population of the green emission level. A power law dependence of the homogeneous linewidths with temperature with an exponent of 1.35 was used to fit our experimental data.

In summary, our results confirm that thermal effects, which determine homogeneous broadening, are responsible for the temperature dependence of the green upconversion emission.

Acknowledgments

The authors gratefully acknowledge J.M. Guerra for providing the cryostat and N. Díaz-Herrera for her expert assistance in fiber splicing. This work has been supported by projects FIS2010-22082 (Ministerio de Ciencia e Innovación) and GR35/10-910133 (Santander-Universidad Complutense de Madrid).

References

[1] F. Auzel, Chem. Rev. 104 (2004) 139.
[2] B.R. Reddy, S.K. Nash-Stevenson, J. Appl. Phys. 76 (1994) 3896.
[3] P. Egger, P. Rogin, T. Riedener, H.U. Güdel, M.S. Wickleder, J. Hulliger, Adv. Mater. 8 (1996) 668.
[4] F. Wang, X. Liu, Chem. Soc. Rev. 38 (2009) 976.
[5] X. Zou, T. Izumitani, J. Non-Cryst. Solid 162 (1993) 68.
[6] R.A. McFarlane, Appl. Phys. Lett. 54 (1989) 2301.
[7] R. Scheps, IEEE J. Quantum Electron. 30 (1994) 2914.
[8] T.J. Whitley, C.A. Millar, R. Wyatt, M.C. Brierley, D. Szebesta, Electron. Lett. 27 (1991) 1785.
[9] D. Piehler, D. Craven, Electron. Lett. 30 (1994) 1759.
[10] D.N. Messias, M.V.D. Vermelho, A.S. Gouveia-Neto, J.S. Aitchison, Rev. Sci. Instrum. 73 (2002) 476.
[11] S.F. Lim, R. Riehn, W.S. Ryu, N. Khanarian, C.-K. Tung, D. Tank, R.H. Austin, Nano Lett. 6 (2006) 169.
[12] D.K. Chatterjee, A.J. Rufaihah, Y. Zhang, Biomaterials 29 (2008) 937.
[13] F. Zhang, G.B. Braun, Y. Shi, Y. Zhang, X. Sun, N.O. Reich, D. Zhao, G. Stucky, J. Am. Chem. Soc. 132 (2010) 2850.
[14] F. Vetrone, R. Naccache, A. Zamarrón, A. Juarranz de la Fuente, F. Sanz-Rodríguez, L. Martinez Maestro, E. Martín Rodríguez, D. Jaque, J. García Solé, J.A. Capobianco, ACS Nano 4 (2010) 3254.
[15] E. Downing, L. Hesselink, J. Ralston, R. Macfarlane, Science 273 (1996) 1185.
[16] A. Shalav, B.S. Richards, T. Trupke, K.W. Krämer, H.U. Güdel, Appl. Phys. Lett. 86 (2005) 013505.
[17] M. Pollnau, D.R. Gamelin, S.R. Lüthi, H.U. Güdel, M.P. Hehlen, Phys. Rev. B 61 (2000) 3337.
[18] J.P. Van der Ziel, F.W. Ostermayer Jr., L.G. Van Uitert, Phys. Rev. B 2 (1970) 4432.
[19] B.R. Reddy, P. Venkateswarlu, Appl. Phys. Lett. 64 (1994) 1327.
[20] W. Jia, K-S. Lim, H. Liu, Y. Wang, J.J. Ju, S.I. Yun, F.E. Fernandez, W.M. Yen, J. Lumin. 66 & 67 (1996) 190.
[21] T. Catunda, L.A.O. Nunes, A. Florez, Y. Messaddeq, M.A. Aegerter, Phys. Rev. B 53 (1996) 6065.
[22] G.S. Maciel, C.B. de Araújo, Y. Messaddeq, M.A. Aegerter, Phys. Rev. B 55 (1997) 6335.
[23] M. Takahashi, M. Shojiya, R. Kanno, Y. Kawamoto, K. Kadono, T. Ohtsuki, N. Peyghambarian, J. Appl. Phys. 81 (1997) 2940.
[24] T. Riedener, H.U. Güdel, J. Chem. Phys. 107 (1997) 2169.
[25] R. Balda, A.J. Garcia-Adeva, M. Voda, J. Fernández, Phys. Rev. B 69 (2004) 205203.
[26] M.V.D. Vermelho, A.S. Gouveia-Neto, H.T. Amorim, F.C. Cassanjes, S.J.L. Ribeiro, Y. Messaddeq, J. Lumin. 102–103 (2003) 755.
[27] S. Golab, W. Ryba-Romanowski, G. Dominiack-Dzik, T. Lukasiewicz, M. Swirkowicz, J. Alloys Compd. 323–324 (2001) 288.
[28] P.V. dos Santos, E.A. Gouveia, M.T. de Araujo, A.S. Gouveia-Neto, A.S.B. Sombra, J.A. Medeiros Neto, Appl. Phys. Lett. 74 (1999) 3607.
[29] M.J. Weber, Phys. Rev. B 8 (1973) 54.
[30] R.M. Macfarlane, R.M. Shelby, J. Lumin. 36 (1987) 179.
[31] E. Desurvire, J.L. Zyskind, J.R. Simpson, IEEE Photon. Technol. Lett. 2 (1990) 246.
[32] J.L. Zyskind, E. Desurvire, J.W. Sulhoff, D.J. Di Giovanni, IEEE Photon. Technol. Lett. 2 (1990) 869.
[33] L. Bigot, A.-M. Jurdyc, B. Jacquier, L. Gasca, D. Bayart, Phys. Rev. B 66 (2002) 214204.
[34] J. Hegarty, M.M. Broer, B. Golding, J.R. Simpson, J.B. MacChesney, Phys. Rev. Lett. 51 (1983) 2033.
[35] M.U. Staudt, S.R. Hastings-Simon, M. Afzelius, D. Jaccard, W. Tittle, N. Gisin, Opt. Commun. 266 (2006) 720.
[36] J. Hegarty, W.M. Yen, Phys. Rev. Lett. 43 (1979) 1126.
[37] R.T. Brundage, W.M. Yen, Phys. Rev. B 33 (1986) 4436.
[38] S. Melle, O.G. Calderón, M.A. Antón, F. Carre no, A. Egatz-Gómez, J. Opt. Soc. Am. B 29 (2012) 2189.
[39] R. Naccache, F. Vetrone, J.C. Boyer, J.A. Capobianco, A. Speghini, M. Bettinelli, G.C. Righini, Mater. Lett. 58 (2004) 2207.
[40] M.P. Hehlen, N.J. Cockroft, T.R. Gosnell, Phys. Rev. B 56 (1997) 9302.
[41] A. Florez, Y. Messaddeq, O.L. Malta, M.A. Aegerter, J. Alloys Compd. 227 (1995) 135.
[42] M.D. Shinn, W.A. Sibley, M.G. Drexhage, R.N. Browns, Phys. Rev. B 27 (1983) 6635.